Hindawi
Mathematical Problems in Engineering
Volume 2018, Article ID 6968526, 13 pages
https://doi.org/10.1155/2018/6968526

Research Article

Constrained Adaptive Neural Control for Air-Breathing Hypersonic Vehicles without Backstepping

Shili Tan, Humin Lei, and Pengfei Wang

Air and Missile Defense College, Air Force Engineering University, Xi'an 710051, China

Correspondence should be addressed to Shili Tan; tanslchn@163.com

Received 29 April 2018; Revised 13 July 2018; Accepted 30 July 2018; Published 6 August 2018

Academic Editor: Javier Moreno-Valenzuela

An adaptive neural control scheme without backstepping is proposed for the air-breathing hypersonic vehicle subject to input constraints. To estimate the unknown nonlinearity of velocity subsystem and altitude subsystem, two radial basis function neural networks (RBFNNs) are constructed. Since the complex backstepping design steps are not needed, the proposed control structure is quite concise and the problem of "explosion of terms" is avoided. Moreover, a novel nonlinear auxiliary system is constructed to solve the problem of input constraints. The advantage of the proposed auxiliary system is that its high-order form has good performance and the parameter tuning is relatively easy. Simulation results show that the designed controllers achieve stable tracking of reference commands with good performance.

1. Introduction

Air-breathing hypersonic vehicle (AHV) has attracted wide concern, because it offers a promising and economic access to near space [1, 2]. The design of the flight control system is an important issue to ensure that the AHV can accomplish its intended task. Due to the complex flight environment, the highly nonlinear dynamic behavior, and the large uncertainty [3, 4], it is a huge challenge to design the controllers with satisfactory performance.

Recently, there are already numerous publications on the design of the flight control system for AHV. A robust linear output-control strategy is investigated for AHV, achieving the stable tracking of reference trajectories [5]. Since the feedback linearization (FL) remains based on the accurate model which is difficult to be obtained, the robustness of FL is weak when there is the model uncertainty. To enhance the robustness with respect to model parameters, a nonfragile control scheme is studied based on the linear parameter-varying (LPV) model [6, 7]. Also the sliding mode control is an effective nonlinear control method and is widely studied for AHV subject to the uncertainty. A key technique for sliding mode control is how to solve the chattering problem [8]. To reduce the chattering, the quasi-continuous high-order mode controllers are exploited, effectively reducing the flutter of the AHV [9]. By introducing the nonlinear disturbance observers (NDO), the total uncertainty is estimated online, and the robustness of the controller is guaranteed [10, 11]. Noticing that the robustness of the designed controllers is closely related to the NDO, an novel NDO based on hyperbolic sine function is investigated and the robustness is enhanced [12]. Moreover, much concern has been on the intelligent controls such as the fuzzy logical system (FLS)[13–15] and the neural network (NN)[16, 17]. The minimal learning parameter (MLP) scheme [13, 14, 16] and the composite learning-based parameter adaptive law [15, 17] are constructed to update the FLS/NN weights. By estimating the model uncertainty accurately and compensating for the controllers, the robustness of the proposed control scheme is ensured.

Backstepping control is regarded as an effective tool to solve the problem of unmatched uncertainty [18, 19]. Noting that the traditional backstepping control needs the tedious analytical calculation of derivatives, the problem of the "explosion of terms" is inevitable. Therefore, the dynamic surface control [20, 21], command filtered approaches [22], and tracking differentiator (TD)[12] are proposed to solve the problem of "explosion of terms". Though good results

in terms of command tracking can be gained by the above method, the whole control system becomes cumbersome and it is unfavorable to the design of the controller. To simplify the design process of the controllers, the controllers without the virtual control laws are creatively designed [16]. However, the expression of the final actual controller becomes complex with a large number of state variables and design parameters. Motivated by the above studies [13, 14, 16, 17], the radial basis function neural networks (RBFNNs) with MLP algorithm are constructed to approximate the model uncertainty. Different from the previous studies, the control scheme without backstepping is proposed by introducing the high-order differentiator. Thus there is no need of complex strict-feedback form and virtual controllers. Also only two RBFNNs are needed to estimate the unknown nonlinearity of velocity subsystem and altitude subsystem, respectively.

From a practical perspective, the control inputs are limited to a certain range. The designed controller without considering the input constraints may suffer performance degradation or even instability appearance. Therefore, it is necessary to take the input constraints into consideration. The Nussbaum function based auxiliary design system is employed for the strict-feedback systems and the nonstrict-feedback systems, preventing the outputs from violating the constraints [23, 24]. Also a linear auxiliary system is adopted for the backstepping scheme [25] and the disturbance observer-based feedback linearization control [26]. Moreover, an novel hybrid auxiliary system is designed to solve the problem of the nonsymmetric nonlinear input constraints [27], and it has been applied to the AHV systems [28, 29] and the flexible spacecraft systems [30]. However, these antiwindup methods can only be applied in some specific control scheme such as the backstepping control. Regardless of the linear auxiliary system [25, 26] or the hybrid auxiliary system [27–30], it is not suitable to be extended to the high-order forms. Since a high-order auxiliary system is required for the altitude subsystem under the proposed control scheme, a novel nonlinear auxiliary system is constructed.

The remainder of the paper is organized as follows: the inputs constrained AHV model and the description of RBFNN are presented in Section 2. Then, the main design process of the controllers is provided in Section 3. Next, Sections 4 and 5 show the stability analysis and simulation, respectively. Finally, the conclusions are summarized in Section 6. The main contributions of this paper are summarized as follows.

(1) Different from the adaptive neural control schemes in [16, 17, 28], there is no need of complex backstepping design steps in this paper. Thus the proposed control structure is quite concise and the problem of "explosion of terms" is avoided.

(2) Compared with the linear auxiliary system [25, 26] and the hybrid auxiliary system [27–30], the nonlinear auxiliary system proposed in this paper can be extended to the high-order forms and applied to the altitude subsystem under the proposed control scheme. Moreover, the parameter tuning for the proposed auxiliary system is relatively easy.

2. Inputs Constrained AHV Model and RBFNN Description

2.1. AHV Model. Based on the X43A aircraft developed by NASA, M. Bolender et al. presented an AHV model [31]. This mode has been widely used in the design of flight control systems. Then, Parker simplified the model by ignoring the weak couplings and slow dynamics [32]. The dynamic equations are formulated as

$$\dot{V} = \frac{1}{m}\left[T\cos\left(\theta-\gamma\right)-D\right]-g\sin\gamma, \tag{1}$$

$$\dot{h} = V\sin\gamma, \tag{2}$$

$$\dot{\gamma} = \frac{1}{mV}\left[L+T\sin\left(\theta-\gamma\right)\right]-\frac{g}{V}\cos\gamma, \tag{3}$$

$$\dot{\theta} = Q, \tag{4}$$

$$I_{yy}\dot{Q} = M+\widetilde{\psi}_1\ddot{\eta}_1+\widetilde{\psi}_2\ddot{\eta}_2, \tag{5}$$

$$k_1\ddot{\eta}_1 = -2\zeta_1\omega_1\dot{\eta}_1-\omega_1^2\eta_1+N_1-\widetilde{\psi}_1\frac{M}{I_{yy}}-\frac{\widetilde{\psi}_1\widetilde{\psi}_2\ddot{\eta}_2}{I_{yy}}, \tag{6}$$

$$k_2\ddot{\eta}_2 = -2\zeta_2\omega_2\dot{\eta}_2-\omega_2^2\eta_2+N_2-\widetilde{\psi}_2\frac{M}{I_{yy}}-\frac{\widetilde{\psi}_2\widetilde{\psi}_1\ddot{\eta}_1}{I_{yy}}, \tag{7}$$

where V, h, γ, θ, and Q denote the velocity, altitude, flight path angle, pitch angle, and pitch rate, respectively. The flexible states $\boldsymbol{\eta} = [\eta_1, \dot{\eta}_1, \eta_2, \dot{\eta}_2]$ are the first two vibrational modes. m is the mass, I_{yy} the moment of inertia, ξ_i the damping ratio, and ω_i the natural frequency. $k_i = 1+\widetilde{\psi}_i/I_{yy}$, with $\widetilde{\psi}_i$ the constrained beam coupling constant for η_i. The thrust T, lift L, drag D, pitching moment M, and generalized forces N_i $(i = 1, 2)$ are given as follows [17]:

$$\begin{aligned}
L &\approx \overline{q}S\left(C_L^{\alpha}\alpha+C_T^{\delta_e}\delta_e+C_L^0\right),\\
D &\approx \overline{q}S\left(C_D^{\alpha^2}\alpha^2+C_D^{\alpha}\alpha+C_D^{\delta_e^2}\delta_e^2+C_D^{\delta_e}\delta_e+C_D^0\right),\\
T &\approx C_T^{\alpha^3}\alpha^3+C_T^{\alpha^2}\alpha^2+C_T^{\alpha}\alpha+C_T^0,\\
M &\approx z_T T+\overline{q}S\overline{c}\left(C_{M,\alpha}^{\alpha^2}\alpha^2+C_{M,\alpha}^{\alpha}\alpha+C_{M,\alpha}^0+c_e\delta_e\right),\\
N_i &= N_i^{\alpha^2}\alpha^2+N_i^{\alpha}\alpha+N_i^{\delta_e}\delta_e+N_i^0, \quad i=1,2,
\end{aligned} \tag{8}$$

with

$$\begin{aligned}
C_T^{\alpha^3} &= \beta_1\left(h,\overline{q}\right)\phi+\beta_2\left(h,\overline{q}\right),\\
C_T^{\alpha^2} &= \beta_3\left(h,\overline{q}\right)\phi+\beta_4\left(h,\overline{q}\right),\\
C_T^{\alpha} &= \beta_5\left(h,\overline{q}\right)\phi+\beta_6\left(h,\overline{q}\right),\\
C_T^0 &= \beta_7\left(h,\overline{q}\right)\phi+\beta_8\left(h,\overline{q}\right),
\end{aligned} \tag{9}$$

$$\overline{q} = \frac{1}{2}\overline{\rho}V^2,$$

$$\overline{\rho} = \overline{\rho}_0\exp\left(-\frac{h-h_0}{h_s}\right), \tag{10}$$

where ϕ and δ_e are the fuel equivalence ratio and the elevator deflection, respectively; S and $\overline{c}$ denote the reference area and the aerodynamic chord, respectively; $\overline{q}$ is the dynamic pressure, $\overline{\rho}$ the air density, and z_T the thrust to moment coupling coefficient.

2.2. Input Constraints. Two inputs of the AHV are $u = [\phi, \delta_e]^T$. In engineering practice, the inputs cannot be any desired values, but must be limited within a certain range. ϕ must be limited to a certain range to ensure the normal operation of the scramjet. Similarly, the limitation of δ_e is determined by the physical structure of the elevator. The above input constraints can be described as

$$\phi = \begin{cases} \phi_{\max}, & \phi_c \geq \phi_{\max} \\ \phi_c, & \phi_{\min} \leq \phi_c \leq \phi_{\max} \\ \phi_{\min}, & \phi_c \leq \phi_{\min} \end{cases} \tag{11}$$

$$\delta_e = \begin{cases} \delta_{e\max}, & \delta_{ec} \geq \delta_{e\max} \\ \delta_{ec}, & \delta_{e\min} \leq \delta_{ec} \leq \delta_{e\max} \\ \delta_{e\min}, & \delta_{ec} \leq \delta_{e\min} \end{cases} \tag{12}$$

where ϕ_c and δ_{ec} are the inputs to be designed; the "max" and "min" denote the maximum and minimum value in the constrained range, respectively.

2.3. Description of RBFNN. The RBFNN has been widely used because it can approximate any continuous function to an arbitrary precision [16, 33]. Assume that the number of RBFNN nodes is $l \geq 1$. The mapping from the input layer $\mathbf{X} \in \Omega \subset \mathbb{R}^n$ to the output layer $y \in R$ is

$$y = \mathbf{W}^{\mathrm{T}} \boldsymbol{\varphi}(\mathbf{X}), \tag{13}$$

where $\mathbf{W} = [w_1, w_2, \ldots, w_l]^{\mathrm{T}} \in \mathbb{R}^l$ denotes the weight vector; $\boldsymbol{\varphi}(\mathbf{X}) = [\varphi_1(\mathbf{X}), \varphi_2(\mathbf{X}), \ldots, \varphi_l(\mathbf{X})]^{\mathrm{T}} \in \mathbb{R}^l$, $\varphi_j(\mathbf{X})$ is chosen as

$$\varphi_j(\mathbf{X}) = \exp\left[-\frac{\left(\mathbf{X} - \boldsymbol{\mu}_j\right)^{\mathrm{T}}\left(\mathbf{X} - \boldsymbol{\mu}_j\right)}{\sigma_j^2}\right], \quad j = 1, 2, \ldots, l \tag{14}$$

where $\boldsymbol{\mu}_j = [\mu_{j1}, \mu_{j2}, \ldots, \mu_{jn}]^{\mathrm{T}}$ denotes the center vector and σ_j is the width vector.

Assume that $F(\mathbf{X}) : \mathbb{R}^n \longrightarrow \mathbb{R}$ is the function to be approximated. There exists $\mathbf{W}^*$ such that

$$F(\mathbf{X}) = \mathbf{W}^{*\mathrm{T}} \boldsymbol{\varphi}(\mathbf{X}) + \varepsilon, \quad |\varepsilon| \leq \overline{\varepsilon}, \ \forall \mathbf{X} \in \Omega_{\mathbf{X}}, \tag{15}$$

where $\mathbf{W}^*$ denotes the ideal weight vector; ε is the approximation error.

3. Controller Design

The control target is selected as developing a controller $u = [\phi, \delta_e]^{\mathrm{T}}$ so that the outputs $y = [V, h]^{\mathrm{T}}$ can follow the reference commands $y_d = [V_d, h_d]^{\mathrm{T}}$. Considering that V is steered by ϕ to a large degree and h is mainly affected by δ_e, we naturally decompose the AHV model into the V-subsystem and the h-subsystem. In what follows, two constrained adaptive neural controllers will be separately designed for the two subsystems such that $V \longrightarrow V_d$ and $h \longrightarrow h_d$.

Step 1 (designing control law for the V-subsystem). The dynamic equation of V-subsystem is described as

$$\dot{V} = f_V + \phi, \tag{16}$$

where $f_V = [T\cos(\theta - \gamma) - D]/m - g\sin\gamma - \phi$ contains large uncertainty and is approximated by one RBFNN:

$$f_V = \mathbf{W}_V^{*\mathrm{T}} \boldsymbol{\varphi}_V(\mathbf{X}_V) + \varepsilon_V, \quad |\varepsilon_V| \leq \overline{\varepsilon}_V, \tag{17}$$

where $W_V^* = [w_{V1}^*, w_{V2}^*, \ldots, w_{Vl_1}^*]^{\mathrm{T}} \in \mathbb{R}^{l_1}$ is the ideal weight vector; $\boldsymbol{\varphi}_V(\mathbf{X}_V) = [\varphi_{V1}(\mathbf{X}_V), \varphi_{V2}(\mathbf{X}_V), \ldots, \varphi_{Vl_1}(\mathbf{X}_V)]^{\mathrm{T}} \in \mathbb{R}^{l_1}$; $\varphi_{Vj}(\mathbf{X}_V)$, $j = 1, 2, \ldots, l_1$ has same formulation to (14); ε_V is the approximation error.

The error between V and V_d is expressed by

$$z_V = V - V_d. \tag{18}$$

Differentiating z_V by time t, we have

$$\dot{z}_V = f_V + \phi - \dot{V}_d. \tag{19}$$

Inspired by the MLP method [13, 14, 16], the neural controller ϕ is designed as

$$\phi = -k_{V1} z_V - k_{V2} \int_0^t z_V(\tau)\, d\tau - \frac{1}{2} z_V \widehat{\lambda}_V \boldsymbol{\varphi}_V^{\mathrm{T}}(\mathbf{X}_V) \boldsymbol{\varphi}_V(\mathbf{X}_V) + \dot{V}_d, \tag{20}$$

where $k_{V1} > 0$, $k_{V2} > 0$ are design parameters; $\lambda_V = \|\mathbf{W}_V^*\|^2$, with the estimation $\widehat{\lambda}_V$. $\widehat{\lambda}_V$ is decided by the adaptive law as follows:

$$\dot{\widehat{\lambda}}_V = \frac{\kappa_V}{2}\left(z_V'\right)^2 \boldsymbol{\varphi}_V^{\mathrm{T}}(\mathbf{X}_V) \boldsymbol{\varphi}_V(\mathbf{X}_V) - 2\widehat{\lambda}_V, \tag{21}$$

where $\kappa_V > 0$ is a design parameter.

Noting that ϕ is constrained as (11), a novel auxiliary system is designed as

$$\dot{\chi}_V = \frac{-l_V |\chi_V|^{\alpha_1} \cdot \operatorname{sign}(\chi_V)}{|\chi_V| + \delta_V} + (\phi - \phi_c), \tag{22}$$

where $l_V > 0$, $\delta_V > 0$, $\alpha_1 > 0$ are design parameters; χ_V is the state variable.

Define the compensated velocity tracking error as

$$z_V' = z_V - \chi_V \tag{23}$$

Differentiating z_V' by time t and invoking (19) and (22), we have

$$\dot{z}_V' = f_V - \dot{V}_d + \frac{l_V |\chi_V|^{\alpha_1} \cdot \operatorname{sign}(\chi_V)}{|\chi_V| + \delta_V} + \phi_c. \tag{24}$$

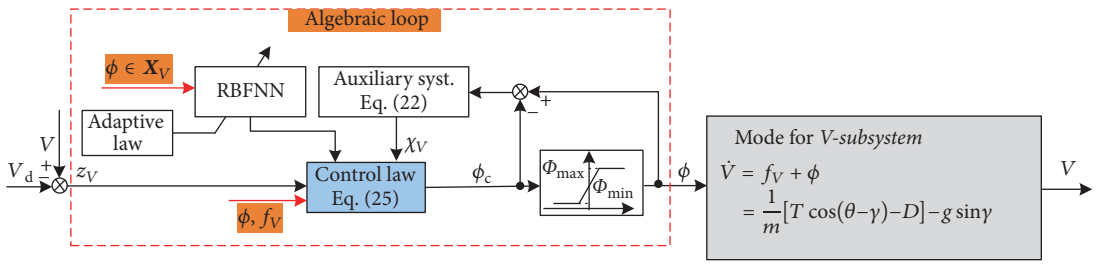

Figure 1: The controller structure of the V-subsystem.

The desired control input ϕ_c is determined by the chosen control law:

$$\phi_c = -k_{V1} z_V' - k_{V2} \int_0^t z_V'(\tau)\, d\tau - \frac{1}{2} z_V' \hat{\lambda}_V \boldsymbol{\varphi}_V^{\mathrm{T}}(\mathbf{X}_V)\, \boldsymbol{\varphi}_V(\mathbf{X}_V) + \dot{V}_d - \frac{l_V |\chi_V|^{\alpha_1} \cdot \mathrm{sign}(\chi_V)}{|\chi_V| + \delta_V}. \tag{25}$$

The controller structure of the V-subsystem is presented in Figure 1.

Remark 1. As shown in Figure 1, if the designed control law ϕ_c directly contains the variable ϕ and f_V, or the RBFNN input layer $\mathbf{X}_V$ contains the element ϕ, the "algebraic loop" problem will appear. Thus, it can be concluded from (25) that the "algebraic loop" problem will not exist as long as $\phi \notin \mathbf{X}_V$.

Step 2 (designing control law for the h-subsystem). The error between h and h_d is defined as

$$z_h = h - h_d. \tag{26}$$

Choose the command of γ as

$$\gamma_d = \arcsin\left(\frac{-k_{h1} z_h - k_{h2} \int_0^t z_h(\tau)\, d\tau + \dot{h}_d}{V}\right). \tag{27}$$

where $k_{h1} > 0$, $k_{h2} > 0$ are design parameters.

According to [33], z_h can converge to zero exponentially, if we choose $\gamma \longrightarrow \gamma_d$. Hence, a constrained adaptive neural controller is developed to steer $\gamma \longrightarrow \gamma_d$.

The dynamic equations of h-subsystem are described as

$$\begin{aligned} \dot{\gamma} &= f_\gamma + \theta, \\ \dot{\theta} &= Q, \\ \dot{Q} &= f_Q + \delta_e, \end{aligned} \tag{28}$$

where $f_\gamma = [L + T\sin(\theta - \gamma)]/(mV) - g\cos(\gamma)/V - \theta$, $f_Q = (M + \tilde{\psi}_1 \ddot{\eta}_1 + \tilde{\psi}_2 \ddot{\eta}_2)/I_{yy} - \delta_e$.

The flight path angle tracking error is given by

$$Z_\gamma = \left(\frac{d}{dt} + \mu\right)^3 \int_0^t z_\gamma(\tau)\, d\tau, \tag{29}$$

where $z_\gamma = \gamma - \gamma_d$, $\mu > 0$ is a chosen constant. Obviously, the tracking error z_γ is bounded only if Z_γ is bounded, because the polynomial $(s + \mu)^3$ is Hurwitz.

Differentiating Z_γ by time t and invoking (28) yields

$$\dot{Z}_\gamma = f_h + \delta_e + 3\mu \ddot{z}_\gamma + 3\mu^2 \dot{z}_\gamma + \mu^3 z_\gamma - \dddot{\gamma}_d, \tag{30}$$

where $f_h = \ddot{f}_\gamma + f_Q$ is highly uncertain and is approached via the following RBFNN:

$$f_h = \mathbf{W}_h^{*\mathrm{T}} \boldsymbol{\varphi}_h(\mathbf{X}_h) + \varepsilon_h, \quad |\varepsilon_h| \le \bar{\varepsilon}_h, \tag{31}$$

where $W_h^* = [w_{h1}^*, w_{h2}^*, \ldots, w_{hl_2}^*]^{\mathrm{T}} \in \mathbb{R}^{l_2}$ is the ideal weight vector; $\boldsymbol{\varphi}_h(\mathbf{X}_h) = [\varphi_{h1}(\mathbf{X}_h), \varphi_{h2}(\mathbf{X}_h), \ldots, \varphi_{hl_2}(\mathbf{X}_h)]^{\mathrm{T}} \in \mathbb{R}^{l_2}$; $\varphi_{hj}(\mathbf{X}_h)$, $j = 1, 2, \ldots, l_2$ has same formulation to (14); ε_h is the approximation error.

Noting that δ_e is constrained as (12), a novel auxiliary system is designed as

$$\begin{aligned} \dot{\chi}_{h,1} &= \chi_{h,2} \\ \dot{\chi}_{h,2} &= \chi_{h,3} \\ \dot{\chi}_{h,3} &= -\frac{l_{h,1} |\chi_{h,1}|^{\alpha_2} \cdot \mathrm{sign}(\chi_{h,1})}{|\chi_{h,1}| + \delta_{h,1}} - \frac{l_{h,2} |\chi_{h,2}|^{\alpha_2} \cdot \mathrm{sign}(\chi_{h,2})}{|\chi_{h,2}| + \delta_{h,2}} - \frac{l_{h,3} |\chi_{h,3}|^{\alpha_2} \cdot \mathrm{sign}(\chi_{h,3})}{|\chi_{h,3}| + \delta_{h,3}} + (\delta_e - \delta_{ec}) \end{aligned} \tag{32}$$

where $l_{h,i} > 0$, $\delta_{h,i} > 0$ $(i = 1, 2, 3)$, and $\alpha_2 \in (0, 1)$ are the design parameters. $\chi_{h,i}$ $(i = 1, 2, 3)$ are the state variables.

The compensated flight path angle tracking error is given by

$$\begin{aligned} z_\gamma' &= z_\gamma - \chi_{h,1} \\ Z_\gamma' &= \left(\frac{d}{dt} + \mu\right)^3 \int_0^t z_\gamma'(\tau)\, d\tau \end{aligned} \tag{33}$$

since

$$\begin{aligned} \dot{z}_\gamma' &= \dot{\gamma} - \dot{\gamma}_d - \chi_{h,2} \\ \ddot{z}_\gamma' &= \ddot{\gamma} - \ddot{\gamma}_d - \chi_{h,3} \end{aligned}$$

$$\ddot{\bar{z}}'_\gamma = f_h + \delta_{ec} - \ddot{\bar{\gamma}}_d + \frac{l_{h,1}\left|\chi_{h,1}\right|^{\alpha_2}\cdot \operatorname{sign}\left(\chi_{h,1}\right)}{\left|\chi_{h,1}\right| + \delta_{h,1}} + \frac{l_{h,2}\left|\chi_{h,2}\right|^{\alpha_2}\cdot \operatorname{sign}\left(\chi_{h,1}\right)}{\left|\chi_{h,2}\right| + \delta_{h,2}} + \frac{l_{h,3}\left|\chi_{h,3}\right|^{\alpha_2}\cdot \operatorname{sign}\left(\chi_{h,1}\right)}{\left|\chi_{h,3}\right| + \delta_{h,3}} \tag{34}$$

Differentiating Z'_γ by time t, we have

$$\dot{Z}'_\gamma = f_h + \delta_{ec} - \ddot{\bar{\gamma}}_d + 3\mu\ddot{\bar{z}}'_\gamma + 3\mu^2\dot{\bar{z}}'_\gamma + \mu^3 z'_\gamma + \frac{l_{h,1}\left|\chi_{h,1}\right|^{\alpha_2}\cdot \operatorname{sign}\left(\chi_{h,1}\right)}{\left|\chi_{h,1}\right| + \delta_{h,1}} + \frac{l_{h,2}\left|\chi_{h,2}\right|^{\alpha_2}\cdot \operatorname{sign}\left(\chi_{h,2}\right)}{\left|\chi_{h,2}\right| + \delta_{h,2}} + \frac{l_{h,3}\left|\chi_{h,3}\right|^{\alpha_2}\cdot \operatorname{sign}\left(\chi_{h,3}\right)}{\left|\chi_{h,3}\right| + \delta_{h,3}} \tag{35}$$

Considering that $\dot{\gamma}$, $\ddot{\gamma}$, $\dot{\gamma}_d$, $\ddot{\gamma}_d$, and $\ddot{\bar{\gamma}}_d$ in (34) cannot be obtained directly, we get their estimations by introducing the finite-time-convergent differentiator [34]. Assume that the estimations are $\hat{\dot{\gamma}}$, $\hat{\ddot{\gamma}}$, $\hat{\dot{\gamma}}_d$, $\hat{\ddot{\gamma}}_d$, and $\hat{\ddot{\bar{\gamma}}}_d$. The estimation errors are defined as

$$\begin{aligned} e_1 &= \hat{\dot{\gamma}} - \dot{\gamma}, \\ e_2 &= \hat{\ddot{\gamma}} - \ddot{\gamma} \\ e_3 &= \hat{\dot{\gamma}}_d - \dot{\gamma}_d, \\ e_4 &= \hat{\ddot{\gamma}}_d - \ddot{\gamma}_d, \\ e_5 &= \hat{\ddot{\bar{\gamma}}}_d - \ddot{\bar{\gamma}}_d \end{aligned} \tag{36}$$

According to [34], there exist positive constants $\bar{e}_i$ such that

$$\left|e_i\right| \le \bar{e}_i, \quad (i = 1, 2, \ldots, 5). \tag{37}$$

The desired control input δ_{ec} is determined by the chosen control law:

$$\delta_{ec} = -k_\gamma Z'_\gamma - \frac{1}{2}Z'_\gamma\widehat{\lambda}_h\boldsymbol{\varphi}_h^{\mathrm{T}}\left(\mathbf{X}_h\right)\boldsymbol{\varphi}_h\left(\mathbf{X}_h\right) - 3\mu\ddot{\bar{z}}'_\gamma - 3\mu^2\dot{\bar{z}}'_\gamma - \mu^3 z'_\gamma + \hat{\ddot{\bar{\gamma}}}_d - \frac{l_{h,1}\left|\chi_{h,1}\right|^{\alpha_2}\cdot \operatorname{sign}\left(\chi_{h,1}\right)}{\left|\chi_{h,1}\right| + \delta_{h,1}} - \frac{l_{h,2}\left|\chi_{h,2}\right|^{\alpha_2}\cdot \operatorname{sign}\left(\chi_{h,2}\right)}{\left|\chi_{h,2}\right| + \delta_{h,2}} - \frac{l_{h,3}\left|\chi_{h,3}\right|^{\alpha_2}\cdot \operatorname{sign}\left(\chi_{h,3}\right)}{\left|\chi_{h,3}\right| + \delta_{h,3}}, \tag{38}$$

where $k_\gamma > 0$ is design parameter; $\widehat{\lambda}_h$ is the approximation of $\lambda_h = \|\mathbf{W}_h^*\|^2$ with the following adaptive law:

$$\dot{\widehat{\lambda}}_h = \frac{\kappa_h}{2}\left(\widehat{Z}'_\gamma\right)^2\boldsymbol{\varphi}_h^{\mathrm{T}}\left(\mathbf{X}_h\right)\boldsymbol{\varphi}_h\left(\mathbf{X}_h\right) - 2\widehat{\lambda}_h, \tag{39}$$

where $\kappa_h > 0$ is design parameter.

Remark 2. **(a)** Different from the backstepping design, by applying the finite-time-convergent differentiator to obtain $\dot{\gamma}$, $\ddot{\gamma}$, $\dot{\gamma}_d$, $\ddot{\gamma}_d$, and $\ddot{\bar{\gamma}}_d$ in the chosen control law δ_{ec}, there is no need of complex strict-feedback form and virtual controller. **(b)** Similarly, the RBFNN input layer $\mathbf{X}_h$ must meet the requirement that $\delta_e \notin \mathbf{X}_h$.

4. Stability Analysis

The stability of the designed auxiliary systems (22) and (32) is illustrated first (i.e., Step 1). Assume that $\phi_{\mathrm{m}} > 0$, $\delta_{em} > 0$ meet $|\phi - \phi_c| \le \phi_m$, $|\delta_e - \delta_{ec}| \le \delta_{em}$. Choose the Lyapunov function as

$$\begin{aligned} Y_1 &= \frac{1}{2}\chi_V^2 \\ Y_2 &= l_{h,2}\int_0^{\chi_{h,1}}\frac{\left|\tau_1\right|^{\alpha_2}\cdot \operatorname{sign}\left(\tau_1\right)}{\left|\tau_1\right| + \delta_{h,1}}d\tau_1 \\ &\quad + l_{h,2}\int_{\chi_{h,1}}^{\chi_{h,2}}\frac{\left|\tau_2\right|^{\alpha_2}\cdot \operatorname{sign}\left(\tau_2\right)}{\left|\tau_2\right| + \delta_{h,2}}d\tau_2 + \frac{\chi_{h,3}^2}{2} \end{aligned} \tag{40}$$

Differentiating Y_1 and Y_2 by time t and invoking (22) and (32) yield

$$\begin{aligned} \dot{Y}_1 &= \chi_V\dot{\chi}_V = \frac{-l_V\left|\chi_V\right|^{\alpha_1+1}}{\left|\chi_V\right| + \delta_V} + \chi_V\left(\phi - \phi_c\right) \\ &\le -\left(l_V\frac{\left|\chi_V\right|^{\alpha_1}}{\left|\chi_V\right| + \delta_V} - \phi_m\right)\left|\chi_V\right|. \\ \dot{Y}_2 &= l_{h,2}\frac{\left|\chi_{h,1}\right|^{\alpha_2}\cdot \operatorname{sign}\left(\chi_{h,1}\right)}{\left|\chi_{h,1}\right| + \delta_{h,1}}\dot{\chi}_{h,1} \\ &\quad + l_{h,2}\left(\frac{\left|\chi_{h,2}\right|^{\alpha_2}\cdot \operatorname{sign}\left(\chi_{h,2}\right)}{\left|\chi_{h,2}\right| + \delta_{h,2}}\dot{\chi}_{h,2} - \frac{\left|\chi_{h,1}\right|^{\alpha_2}\cdot \operatorname{sign}\left(\chi_{h,1}\right)}{\left|\chi_{h,1}\right| + \delta_{h,1}}\dot{\chi}_{h,1}\right) + \chi_{h,3}\dot{\chi}_{h,3} = \chi_{h,3}\left(\delta_e\right. \\ &\quad \left. - \delta_{ec}\right) - \left(\frac{l_{h,1}\left|\chi_{h,1}\right|^{\alpha_2}\cdot \operatorname{sign}\left(\chi_{h,1}\right)}{\left|\chi_{h,1}\right| + \delta_{h,1}}\right. \\ &\quad \left. + \frac{l_{h,3}\left|\chi_{h,3}\right|^{\alpha_2}\cdot \operatorname{sign}\left(\chi_{h,3}\right)}{\left|\chi_{h,3}\right| + \delta_{h,3}}\right)\chi_{h,3} \le \chi_{h,3}\delta_{em} \\ &\quad - \frac{l_{h,1}\left|\chi_{h,1}\right|^{\alpha_2}\cdot \operatorname{sign}\left(\chi_{h,1}\right)}{\left|\chi_{h,1}\right| + \delta_{h,1}}\chi_{h,3} \end{aligned} \tag{41}$$

$$-\frac{l_{h,3}\left|\chi_{h,3}\right|^{\alpha_2}\cdot\operatorname{sign}\left(\chi_{h,3}\right)}{\left|\chi_{h,3}\right|+\delta_{h,3}}\chi_{h,3}$$
$$\leq-\left(\frac{l_{h,1}\left|\chi_{h,1}\right|^{\alpha_2}\cdot\operatorname{sign}\left(\chi_{h,1}\right)}{\left|\chi_{h,1}\right|+\delta_{h,1}}-\delta_{em}\right)\left|\chi_{h,3}\right| \tag{42}$$

Note that the following inequality holds:

$$\frac{\left|\chi_V\right|^{\alpha_1}}{\left|\chi_V\right|+\delta_V}\leq\eta_V,\quad\alpha_1\in(0,1], \tag{43}$$

$$\frac{l_{h,1}\left|\chi_{h,1}\right|^{\alpha_2}\cdot\operatorname{sign}\left(\chi_{h,1}\right)}{\left|\chi_{h,1}\right|+\delta_{h,1}}\leq\eta_{h,1},\quad\alpha_2\in(0,1], \tag{44}$$

where $\eta_V>0$ and $\eta_{h,1}>0$ are constants.

There exist $l_V>\phi_m/\eta_V$ and $l_{h,1}>\delta_{em}/\eta_{h,1}$ such that $\dot{Y}_1<0$ and $\dot{Y}_2<0$. According to Lyapunov theory, states χ_V, $\chi_{h,1}$, $\chi_{h,2}$, and $\chi_{h,3}$ are bounded and can converge to zero in finite time by setting bounded $\chi_V(0)$, $\chi_{h,1}(0)$, $\chi_{h,2}(0)$, and $\chi_{h,3}(0)$.

Then, we illustrate the stability of the closed-loop system consisting of the plant (1)~(7) and controllers (25) and (38), (i.e., Step 2). For the V-subsystem, the Lyapunov function is selected as

$$Y_V=\frac{\left(z_V'\right)^2}{2}+\frac{k_{V2}}{2}\left(\int_0^t z_V'(\tau)\,d\tau\right)^2+\frac{\left(\widetilde{\lambda}_V\right)^2}{2\kappa_V}, \tag{45}$$

where $\widetilde{\lambda}_V=\widehat{\lambda}_V-\lambda_V$.

Substituting (17) and (25) into (24), we have

$$\dot{z}_V'=-k_{V1}z_V'-k_{V2}\int_0^t z_V'(\tau)\,d\tau+\mathbf{W}_V^{*\mathrm{T}}\boldsymbol{\varphi}_V(\mathbf{X}_V)$$
$$-\frac{1}{2}z_V'\widehat{\lambda}_V\boldsymbol{\varphi}_V^{\mathrm{T}}(\mathbf{X}_V)\boldsymbol{\varphi}_V(\mathbf{X}_V)+\varepsilon_V. \tag{46}$$

Invoking (21) and (46), the time derivative of Y_V is

$$\dot{Y}_V=z_V'\dot{z}_V'+k_{V2}z_V'\int_0^t z_V'(\tau)\,d\tau+\frac{1}{\kappa_V}\widetilde{\lambda}_V\dot{\widehat{\lambda}}_V$$
$$=-k_{V1}\left(z_V'\right)^2+z_V'\mathbf{W}_V^{*\mathrm{T}}\boldsymbol{\varphi}_V(\mathbf{X}_V)+z_V'\varepsilon_V-\frac{2\widetilde{\lambda}_V\widehat{\lambda}_V}{\kappa_V}$$
$$-\frac{1}{2}\left(z_V'\right)^2\lambda_V\boldsymbol{\varphi}_V^{\mathrm{T}}(\mathbf{X}_V)\boldsymbol{\varphi}_V(\mathbf{X}_V). \tag{47}$$

Since

$$z_V'\mathbf{W}_V^{*\mathrm{T}}\boldsymbol{\varphi}_V(\mathbf{X}_V)\leq\frac{\left(z_V'\right)^2}{2}\left\|\mathbf{W}_V^{*\mathrm{T}}\boldsymbol{\varphi}_V(\mathbf{X}_V)\right\|^2+\frac{1}{2}$$
$$=\frac{\left(z_V'\right)^2}{2}\left\|\mathbf{W}_V^{*}\right\|^2\left\|\boldsymbol{\varphi}_V(\mathbf{X}_V)\right\|^2+\frac{1}{2}, \tag{48}$$

$$z_V'\varepsilon_V\leq\frac{1}{2}\left(z_V'\right)^2\bar{\varepsilon}_V^2+\frac{1}{2}, \tag{49}$$

$$-\frac{2\widetilde{\lambda}_V\widehat{\lambda}_V}{\kappa_V}\leq\frac{\lambda_V^2-\widetilde{\lambda}_V^2}{\kappa_V}\leq\frac{\lambda_V^2}{\kappa_V}, \tag{50}$$

we obtain

$$\dot{Y}_V\leq-\left(k_{V1}-\frac{1}{2}\bar{\varepsilon}_V^2\right)\left(z_V'\right)^2+\frac{1}{\kappa_V}\lambda_V^2+1. \tag{51}$$

For the *h-subsystem*, the Lyapunov function is selected as

$$Y_h=\frac{1}{2}\left(Z_\gamma'\right)^2+\frac{\left(\widetilde{\lambda}_h\right)^2}{2\kappa_h}. \tag{52}$$

where $\widetilde{\lambda}_h=\widehat{\lambda}_h-\lambda_h$.

Combining (31), (35) and (38), we obtain

$$\dot{\widehat{Z}}_\gamma'=-k_\gamma Z_\gamma'+\mathbf{W}_h^{*\mathrm{T}}\boldsymbol{\varphi}_h(\mathbf{X}_h)$$
$$-\frac{1}{2}Z_\gamma'\widehat{\lambda}_h\boldsymbol{\varphi}_h^{\mathrm{T}}(\mathbf{X}_h)\boldsymbol{\varphi}_h(\mathbf{X}_h)+\varepsilon_h. \tag{53}$$

Invoking (39) and (53), the time derivative of Y_h is

$$\dot{Y}_h=Z_\gamma'\dot{Z}_\gamma'+\widetilde{\lambda}_h\dot{\widehat{\lambda}}_h$$
$$=-k_\gamma\left(Z_\gamma'\right)^2+Z_\gamma'\mathbf{W}_h^{*\mathrm{T}}\boldsymbol{\varphi}_h(\mathbf{X}_h)+Z_\gamma'\varepsilon_h-\frac{2\widetilde{\lambda}_h\widehat{\lambda}_h}{\kappa_h}$$
$$-\frac{\left(Z_\gamma'\right)^2}{2}\lambda_h\boldsymbol{\varphi}_h^{\mathrm{T}}(\mathbf{X}_h)\boldsymbol{\varphi}_h(\mathbf{X}_h). \tag{54}$$

Since

$$Z_\gamma'\mathbf{W}_h^{*\mathrm{T}}\boldsymbol{\varphi}_h(\mathbf{X}_h)\leq\frac{\left(Z_\gamma'\right)^2}{2}\left\|\mathbf{W}_h^{*}\right\|^2\left\|\boldsymbol{\varphi}_h(\mathbf{X}_h)\right\|^2+\frac{1}{2}, \tag{55}$$

$$Z_\gamma'\varepsilon_h\leq\frac{1}{2}\left(Z_\gamma'\right)^2\bar{\varepsilon}_h^2+\frac{1}{2}, \tag{56}$$

$$-\frac{2\widetilde{\lambda}_h\widehat{\lambda}_h}{\kappa_h}\leq\frac{\lambda_h^2-\widetilde{\lambda}_h^2}{\kappa_h}\leq\frac{\lambda_h^2}{\kappa_h}, \tag{57}$$

we obtain

$$\dot{Y}_h\leq-\left(k_\gamma-\frac{1}{2}\bar{\varepsilon}_h^2\right)\left(Z_\gamma'\right)^2+\frac{1}{\kappa_h}\lambda_h^2+1. \tag{58}$$

For the closed-loop control system consisting of the plant (1)~(7) and controllers (25) and (38), the Lyapunov function candidate is selected as follows:

$$Y_3=Y_V+Y_h \tag{59}$$

Taking time derivative along (59), we have

$$\dot{Y}_3=\dot{Y}_V+\dot{Y}_h$$
$$\leq-\left(k_{V1}-\frac{1}{2}\bar{\varepsilon}_V^2\right)\left(z_V'\right)^2-\left(k_\gamma-\frac{1}{2}\bar{\varepsilon}_h^2\right)\left(Z_\gamma'\right)^2+\Sigma \tag{60}$$

where $\Sigma=(1/\kappa_V)\lambda_V^2+(1/\kappa_h)\lambda_h^2+2$.

Table 1: States initialization.

Item	Value	Unit
V	8200	ft/s
h	88600	ft
γ	0	deg
θ	1.5295	deg
Q	0	deg/s
η_1	0.9374	-
$\dot{\eta}_1$	0	-
η_2	0.7709	-
$\dot{\eta}_2$	0	-

Choosing $k_{V1} > \bar{\varepsilon}_V^2/2$ and $k_\gamma > \bar{\varepsilon}_h^2/2$, the compact sets are expressed by

$$\Omega_{z_V'} = \left\{ z_V' \,\middle|\, \left|z_V'\right| \le \sqrt{\frac{\Sigma}{\left(k_{V1} - (1/2)\,\bar{\varepsilon}_V^2\right)}} \right\}. \tag{61}$$

$$\Omega_{\widehat{Z}_\gamma'} = \left\{ Z_\gamma' \,\middle|\, \left|Z_\gamma'\right| \le \sqrt{\frac{\Sigma}{\left(k_\gamma - (1/2)\,\bar{\varepsilon}_h^2\right)}} \right\}. \tag{62}$$

The radiuses of $\Omega_{z_V'}$ and $\Omega_{\widehat{Z}_\gamma'}$ can be arbitrarily small by choosing enough large k_{V1}, k_γ. Besides, $\dot{Y}_3$ is negative when $z_V' \notin \Omega_{z_V'}$, $\widehat{Z}_\gamma' \notin \Omega_{\widehat{Z}_\gamma'}$. Thus, z_V' and Z_γ' can be arbitrarily small. According to (33), the compensated tracking error z_γ' can be arbitrarily small since $\mu > 0$.

Assume that the upper bounds of χ_V, $\chi_{h,1}$ are positive constants χ_V^M, $\chi_{h,1}^M$, respectively. From (23) and (33), we have

$$\begin{aligned} \left|z_V\right| &= \left|z_V' + \chi_V\right| \le \left|z_V'\right| + \chi_V^M \\ \left|z_\gamma\right| &= \left|+\chi_{h,1}\right| \le \left|z_\gamma'\right| + \chi_{h,1}^M \end{aligned} \tag{63}$$

The tracking errors z_V and z_γ are bounded. Therefore, the proposed control scheme can make $V \longrightarrow V_d$ and $\gamma \longrightarrow \gamma_d$. Furthermore, we obtain $h \longrightarrow h_d$.

5. Simulation Results

The aerodynamic parameters and physical properties of the AHV model are given in Tables 2–6. To characterize model uncertainty (including parameter uncertainties and external disturbances), we add the perturbation into the nominal aerodynamic coefficient. Define the actual coefficient as

$$C = C_0\left[1 + \Delta C \sin\left(0.05\pi t\right)\right], \tag{64}$$

where C_0 represents the nominal value and ΔC denotes the amplitude of coefficient perturbation.

The states initialization of the AHV are given in Table 1.

The reference commands V_d and h_d are obtained through a second-order system with a natural frequency $\omega_n = 0.1$ and a damping coefficient $\varsigma = 0.9$. The velocity steps are from 8200 ft/s to 8800 ft/s and the altitude steps from 88600 ft to 89200 ft.

Table 2: Miscellaneous coefficient values.

Coefficient	Value	Units
S	1.7000×10^1	$\text{ft}^2 \bullet \text{ft}^{-1}$
ρ_0	6.7429×10^{-5}	$\text{slugs} \bullet \text{ft}^{-3}$
h_0	8.5000×10^4	ft
h_s	2.1358×10^4	ft
m	3.0000×10^2	$\text{lb} \bullet \text{ft}^{-1}$
g	3.2000×10^1	$\text{ft} \bullet \text{s}^{-2}$
I_{yy}	5.0000×10^5	$\text{lb} \bullet \text{ft}$

Table 3: Lift and drag coefficient values.

Coefficient	Value	Units
C_L^α	4.6773×10^0	rad^{-1}
$C_T^{\delta_e}$	7.6224×10^{-1}	rad^{-1}
C_L^0	-1.8714×10^{-2}	–
$C_D^{\alpha^2}$	5.8224×10^0	rad^{-2}
C_D^α	-4.5315×10^{-2}	rad^{-1}
$C_D^{\delta_e^2}$	8.1993×10^{-1}	rad^{-2}
$C_D^{\delta_e}$	2.7669×10^{-4}	rad^{-1}
C_D^0	1.0131×10^{-2}	–

Table 4: Moment coefficient values.

Coefficient	Value	Units
z_T	8.3600×10^0	ft
$\bar{c}$	1.7000×10^1	ft
$C_{M,\alpha}^{\alpha^2}$	6.2926×10^0	rad^{-2}
$C_{M,\alpha}^\alpha$	2.1335×10^0	rad^{-1}
$C_{M,\alpha}^0$	1.8979×10^{-1}	–
c_e	-1.2897×10^0	rad^{-1}

Table 5: Thrust coefficient values.

Coefficient	Value	Units
β_1	-3.7693×10^5	$\text{lb} \bullet \text{ft}^{-1} \bullet \text{rad}^{-3}$
β_2	-3.7225×10^4	$\text{lb} \bullet \text{ft}^{-1} \bullet \text{rad}^{-3}$
β_3	2.6814×10^4	$\text{lb} \bullet \text{ft}^{-1} \bullet \text{rad}^{-2}$
β_4	-1.7277×10^4	$\text{lb} \bullet \text{ft}^{-1} \bullet \text{rad}^{-2}$
β_5	3.5542×10^4	$\text{lb} \bullet \text{ft}^{-1} \bullet \text{rad}^{-1}$
β_6	-2.4216×10^3	$\text{lb} \bullet \text{ft}^{-1} \bullet \text{rad}^{-1}$
β_7	6.3785×10^3	$\text{lb} \bullet \text{ft}^{-1}$
β_8	-1.0090×10^2	$\text{lb} \bullet \text{ft}^{-1}$

Choose the design parameters as follows: $k_{V1} = 0.3, k_{V2} = 0.8$, $k_{h1} = 2$, $k_{h2} = 0.1$, $k_\gamma = 50$, $\mu = 1$, $\alpha_1 = \alpha_2 = 0.9$, $l_V = 1$, $\delta_V = 0.1$, $l_{h,1} = 0.5$, $l_{h,2} = l_{h,3} = 1$,, $\delta_{h,i} = 0.1$ $(i = 1, 2, 3)$, $\kappa_V = \kappa_h = 0.05$. The inputs of RBFNNs ((17), (31)) are chosen as $\mathbf{X}_V = [V, \dot{V}_d]^{\mathrm{T}}$, $\mathbf{X}_h = [\gamma, \theta, Q, \dot{\gamma}_d]^{\mathrm{T}}$, and the node numbers are selected as $l_1 = l_2 = 20$. The center vectors $\boldsymbol{\mu}_V$, $\boldsymbol{\mu}_h$ are evenly distributed and the width vectors are set as $\sigma_V = \sigma_f\sqrt{1/l_1}\|\mathbf{V}_V - \boldsymbol{\mu}_V\|_2$, $\sigma_h = \sigma_f\sqrt{1/l_2}\|\mathbf{V}_h - \boldsymbol{\mu}_h\|_2$ with the regulating parameter $\sigma_f = 0.5$.

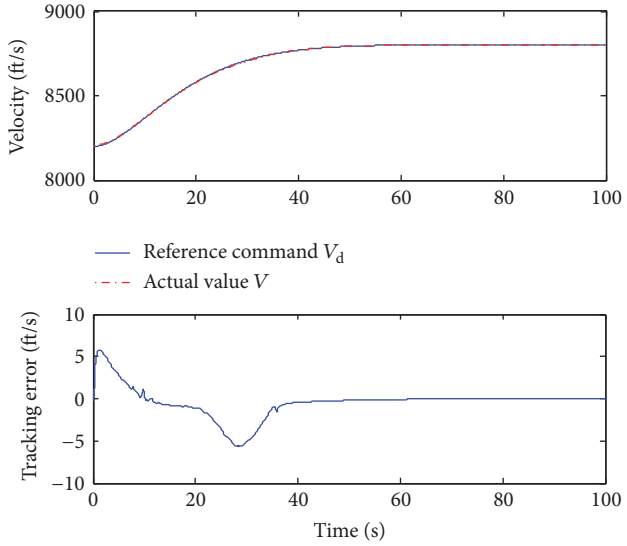

Figure 2: Velocity tracking.

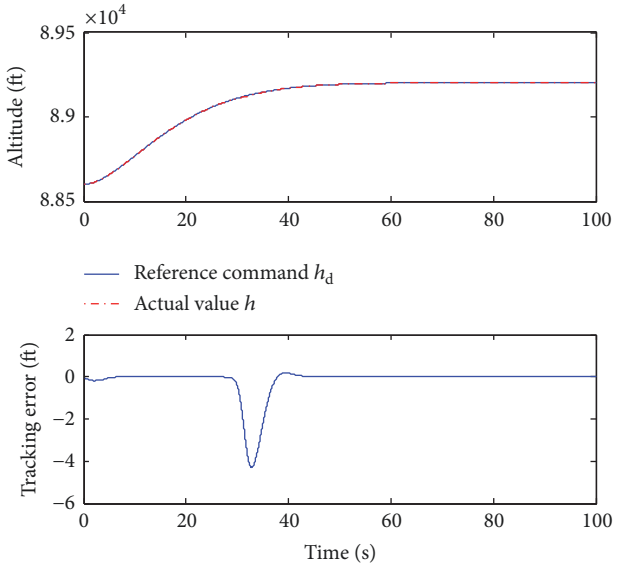

Figure 3: Altitude tracking.

Table 6: N_1 and N_2 coefficient values.

Coefficient	Value	Units
$N_1^{\alpha^2}$	1.4013×10^3	lb • ft^{-1} • slug$^{-0.5}$ • rad^{-2}
N_1^{α}	4.5737×10^3	lb • ft^{-1} • slug$^{-0.5}$ • rad^{-1}
$N_1^{\delta_e}$	1.1752×10^3	lb • ft^{-1} • slug$^{-0.5}$ • rad^{-1}
N_1^0	0.0000×10^1	lb • ft^{-1} • slug$^{-0.5}$
$N_2^{\alpha^2}$	-5.0227×10^3	lb • ft^{-1} • slug$^{-0.5}$ • rad^{-2}
N_2^{α}	2.8633×10^3	lb • ft^{-1} • slug$^{-0.5}$ • rad^{-1}
$N_2^{\delta_e}$	1.2465×10^3	lb • ft^{-1} • slug$^{-0.5}$ • rad^{-1}
N_2^0	-4.4201×10^1	lb • ft^{-1} • slug$^{-0.5}$

Scenario 1. To illustrate the effect of the designed auxiliary systems, the comparative simulations are conducted as follows.

Case I. The input constraints are $\phi \in [0.05, 1.1]$, $\delta_e \in [-18^\circ, 18^\circ]$, and the aerodynamic coefficient perturbation is $\Delta C = 40\%$. Simulation results are presented in Figures 2–9.

Case II. All simulation conditions remain the same except that the auxiliary systems ((22) and (32)) do not work. For the designed controllers without the auxiliary systems, simulation results are shown in Figures 10–14.

Figures 2 and 3 depict the tracking performance that $V \longrightarrow V_d$ and $h \longrightarrow h_d$. It is shown that the outputs V and h steadily track the reference commands with the satisfactory tracking error. The states γ, θ, Q, and the flexible states, as shown in Figures 4 and 5, change smoothly without the chattering and mutation during the entire simulation process. Figures 6–8 depict the inputs and the states of the auxiliary systems. It is obvious that the auxiliary systems compensate for the inputs when the actuators are saturated. Figure 9 shows that the estimations of λ_V and λ_h are bounded and smooth.

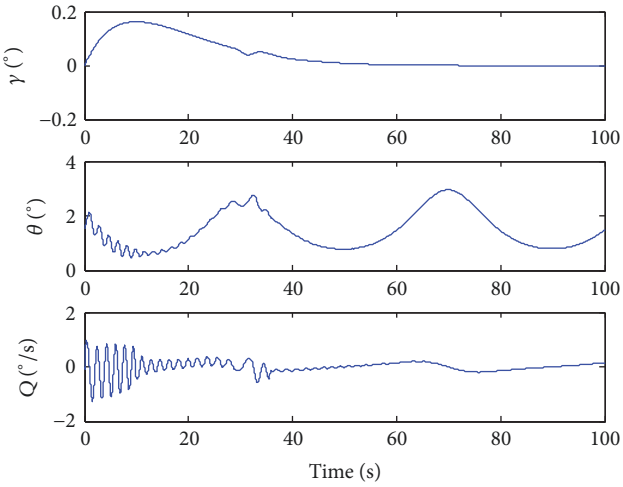

Figure 4: Responses of γ, θ, and Q.

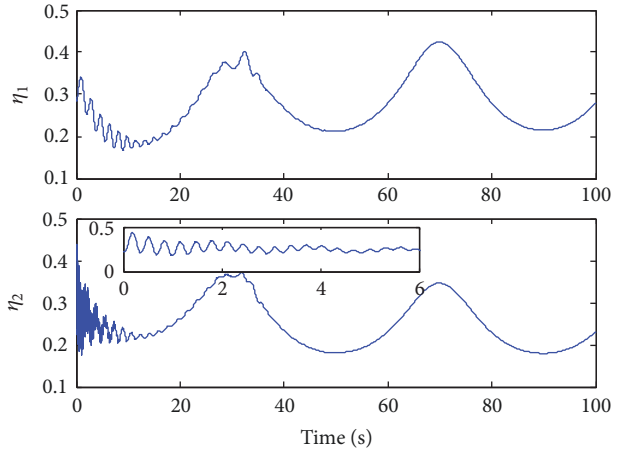

Figure 5: Flexible states.

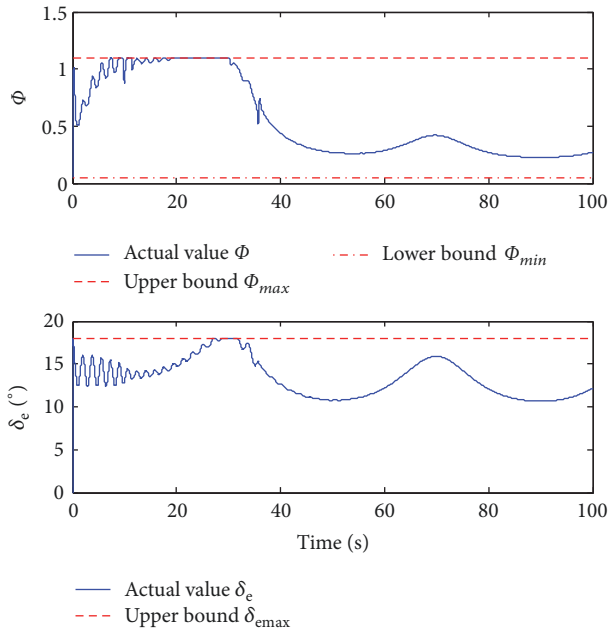

Figure 6: Control inputs.

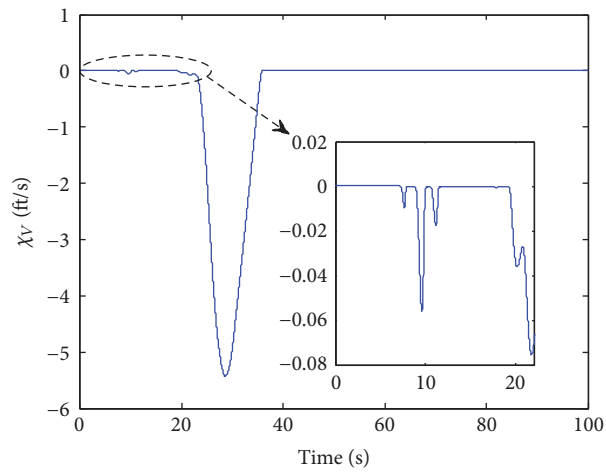

Figure 7: Response of χ_V.

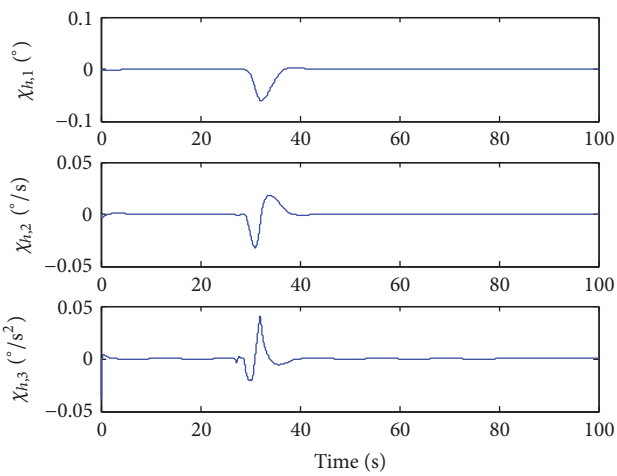

Figure 8: Response of $\chi_{h,1}$, $\chi_{h,2}$, and $\chi_{h,3}$.

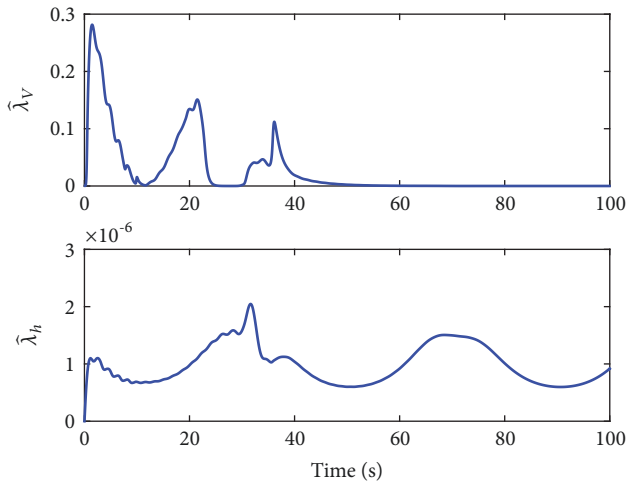

Figure 9: Estimations of λ_V and λ_h.

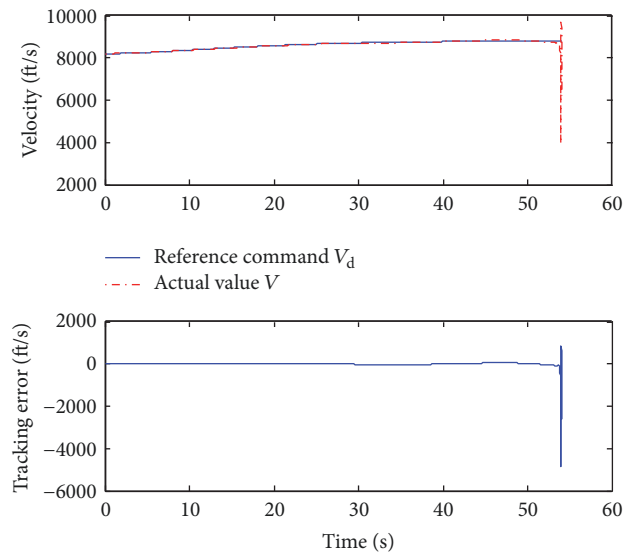

Figure 10: Velocity tracking.

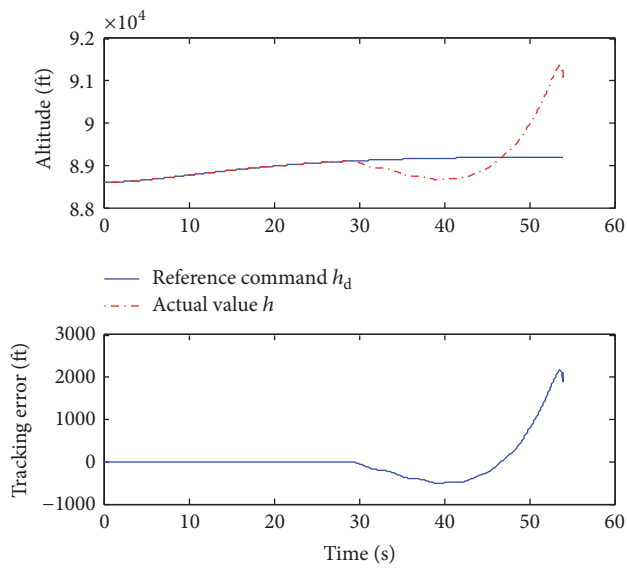

Figure 11: Altitude tracking.

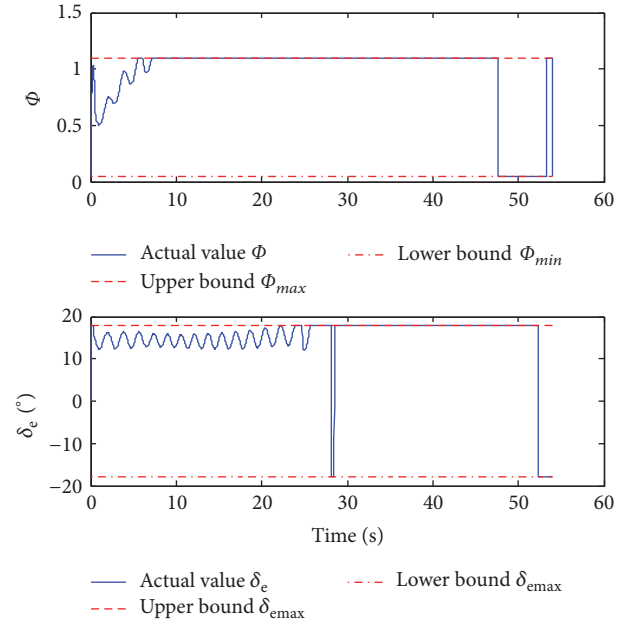

Figure 12: Control inputs.

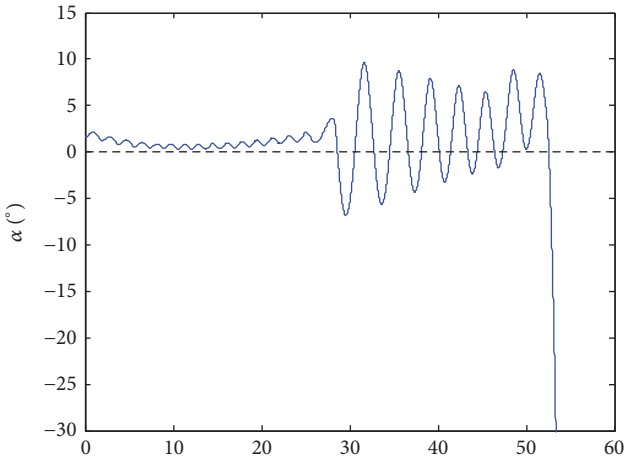

Figure 13: Angle of attack.

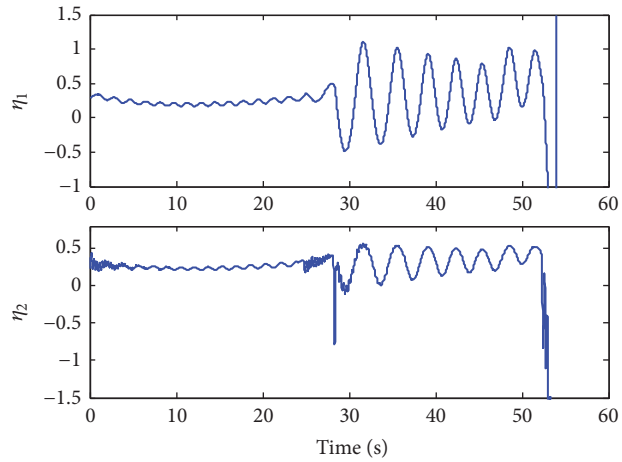

Figure 14: Flexible states.

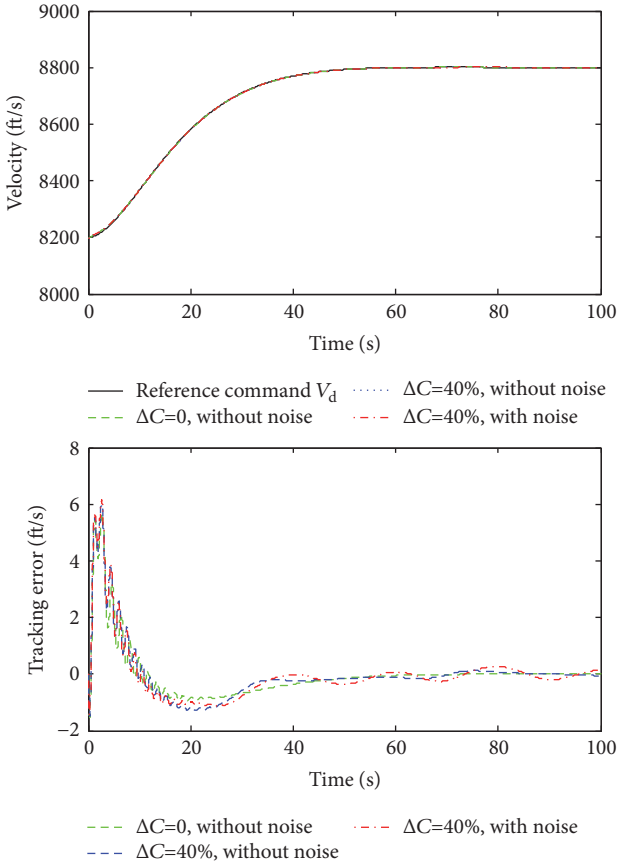

Figure 15: Velocity tracking.

As shown in Figures 10–12, the velocity and altitude become divergent because the control inputs hit their saturation for a long time. It can be observed from Figure 13 that the angle of attack oscillates near zero when the elevator deflection is constrained. Negative angle of attack will directly lead to engine flameout. Figure 14 reveals that the flexible states become divergent, and the aircraft will disintegrate by violent vibration. In conclusion, the designed controllers without the auxiliary systems fail to achieve the tracking of reference commands.

Scenario 2. To show the robustness and effectiveness of the proposed algorithm, the cases are considered as follows.

Case I. Simulations with and without parameter uncertainties and external disturbances are included and compared. The aerodynamic coefficient perturbations are selected as $\Delta C = 40\%$ and $\Delta C = 0$, respectively.

Case II. To show how the proposal works under a noisy environment, the quantization errors in the state variables are described as $V_{error} = 0.6\times\sin(0.1\pi t)$, $h_{error} = 0.2\times\sin(0.1\pi t)$, $Q_{error} = 0.1 \times \pi/180 \times \sin(0.1\pi t)$. In addition, the control input signals are added with the white noise whose mean is 0 and variance is 0.01. Also the aerodynamic coefficient perturbations are selected as $\Delta C = 40\%$.

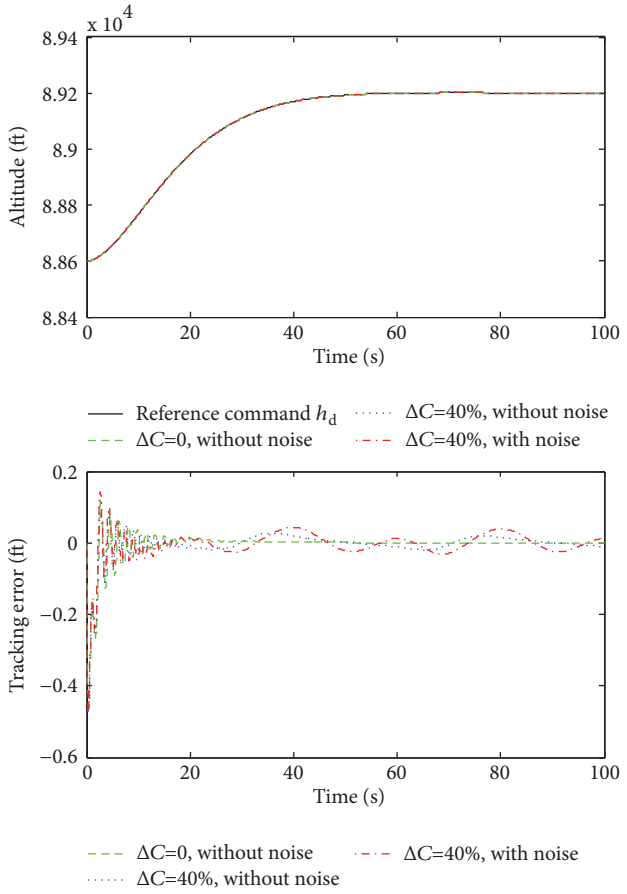

Figure 16: Altitude tracking.

Case III. The backstepping control scheme based on novel NDO in [12] is selected for comparison with the proposed controller in this article. All simulation conditions remain the same as ***Case II***.

In order to ensure the fairness of the comparison, the input constraints are not considered. Simulation results in ***Case I*** and ***Case II*** are shown in Figures 15 and 16 and simulation results in ***Case****III* are presented in Figures 17–20.

From Figures 15-16, it can be seen that the proposed control scheme achieved robust tracking of the velocity and altitude under the environment of parameter uncertainties and additive noise. Figures 17 and 18 reveal that the control method proposed in this article has higher accuracy in the velocity and altitude tracking, compared with the method in [12]. It can be observed from Figures 19 and 20 that the inputs of the method in [12] cannot be adjusted in time, especially in the initial time period, resulting in the flight-path angle, pitch angle, and pitch rate not meeting the requirements of the tracking task.

6. Conclusions

A constrained adaptive neural control without backstepping is proposed for the AHV in this article. It is shown that the proposed control structure is quite concise and the problem of "explosion of terms" is avoided. By conducting the

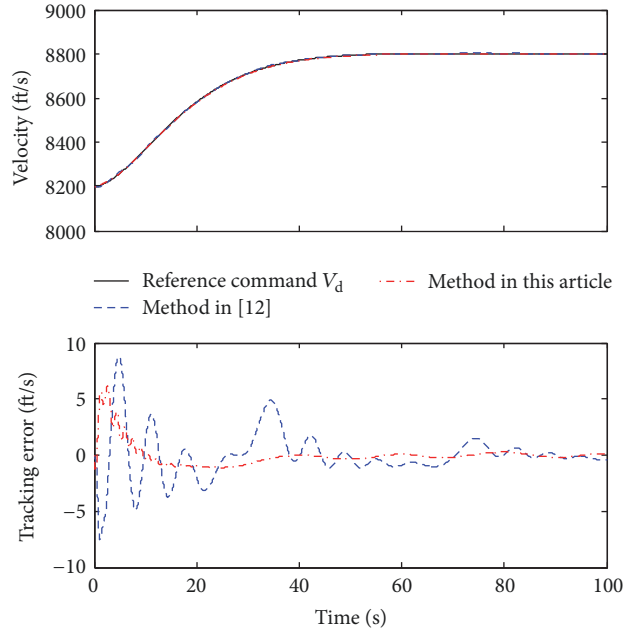

Figure 17: Velocity tracking.

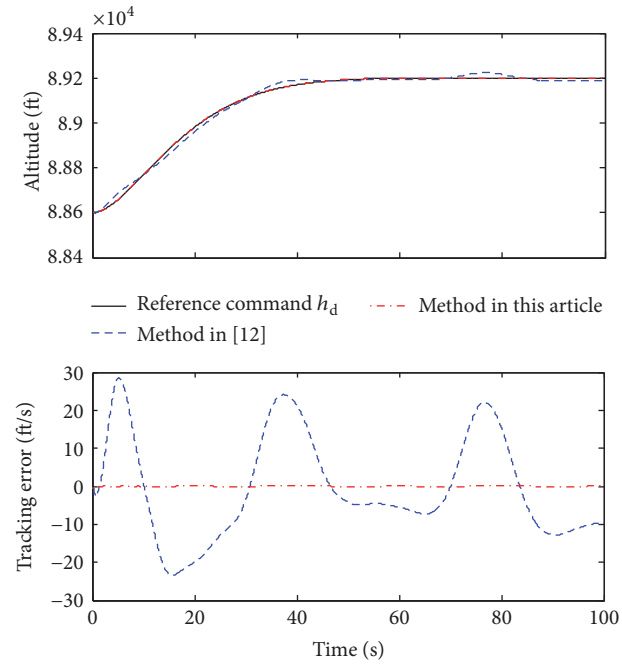

Figure 18: Altitude tracking.

comparative simulations, the effectiveness of the proposed nonlinear auxiliary systems is verified. Compared with the backstepping control scheme based on novel NDO, the proposed algorithm has stronger robustness. Our further works will concentrate on designing better learning algorithms for RBFNN.

Data Availability

The data used in this paper are mainly made of the geometrical parameters, aerodynamic coefficients, and thrust

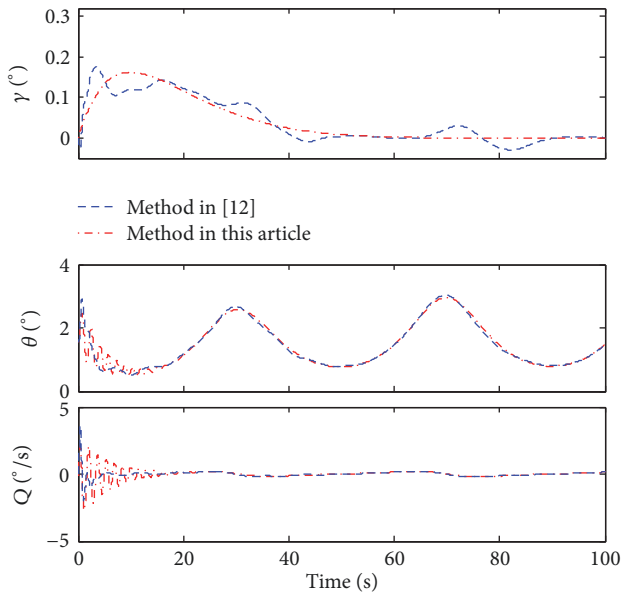

Figure 19: Responses of γ, θ, and Q.

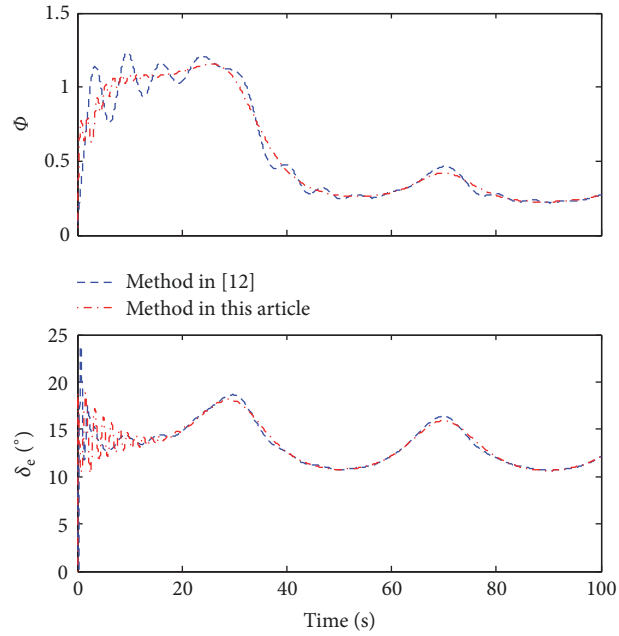

Figure 20: Control inputs.

coefficients for the air-breathing hypersonic vehicle (AHV). Readers can get this data in [32].

Conflicts of Interest

The authors state that the publication of this article does not involve conflicts of interest.

Acknowledgments

This study was cosupported by the National Natural Science Foundation of China (Grants no. 61573374 and no. 61503408) and Aeronautical Science Foundation of China (Grant no. 20150196006).

References

[1] B. Xu, C. Yang, and Y. Pan, "Global neural dynamic surface tracking control of strict-feedback systems with application to hypersonic flight vehicle," *IEEE Transactions on Neural Networks and Learning Systems*, 2015.

[2] L. Fiorentini and A. Serrani, "Adaptive restricted trajectory tracking for a non-minimum phase hypersonic vehicle model," *Automatica*, vol. 48, no. 7, pp. 1248–1261, 2012.

[3] P. Li, X. Yu, Y. Zhang, and X. Peng, "Adaptive Multivariable Integral TSMC of a Hypersonic Gliding Vehicle with Actuator Faults and Model Uncertainties," *IEEE/ASME Transactions on Mechatronics*, 2017.

[4] P. Li, J. Ma, and Z. Zheng, "Disturbance-observer-based fixed-time second-order sliding mode control of an air-breathing hypersonic vehicle with actuator faults," *Proceedings of the Institution of Mechanical Engineers, Part G: Journal of Aerospace Engineering*, vol. 232, no. 2, pp. 344–361, 2016.

[5] D. O. Sigthorsson, P. Jankovsky, A. Serrani, S. Yurkovich, M. A. Bolender, and D. B. Doman, "Robust linear output feedback control of an airbreathing hypersonic vehicle," *Journal of Guidance, Control, and Dynamics*, vol. 31, no. 4, pp. 1052–1066, 2008.

[6] L. G. Wu, X. B. Yang, and F. B. Li, "Nonfragile output tracking control of hypersonic air-breathing vehicles with an LPV model," *IEEE/ASME Transactions on Mechatronics*, vol. 18, no. 4, pp. 1280–1288, 2013.

[7] Y. Huang, C. Sun, C. Qian, and L. Wang, "Non-fragile switching tracking control for a flexible air-breathing hypersonic vehicle based on polytopic LPV model," *Chinese Journal of Aeronautics*, vol. 26, no. 4, pp. 948–959, 2013.

[8] S. Xingling and W. Honglun, "Sliding mode based trajectory linearization control for hypersonic reentry vehicle via extended disturbance observer," *ISA Transactions®*, vol. 53, no. 6, pp. 1771–1786, 2014.

[9] Y. Zhang, R. Li, T. Xue, Z. Liu, and Z. Yao, "An analysis of the stability and chattering reduction of high-order sliding mode tracking control for a hypersonic vehicle," *Information Sciences*, vol. 348, pp. 25–48, 2016.

[10] G. Gao and J. Z. Wang, "Reference command tracking control for an air-breathing hypersonic vehicle with parametric uncertainties," *Journal of The Franklin Institute*, vol. 350, no. 5, pp. 1155–1188, 2013.

[11] G. Wu and X. Meng, "Nonlinear disturbance observer based robust backstepping control for a flexible air-breathing hypersonic vehicle," *Aerospace Science and Technology*, vol. 54, pp. 174–182, 2016.

[12] X. Bu, X. Wu, R. Zhang, Z. Ma, and J. Huang, "Tracking differentiator design for the robust backstepping control of a flexible air-breathing hypersonic vehicle," *Journal of The Franklin Institute*, vol. 352, no. 4, pp. 1739–1765, 2015.

[13] P. F. Wang, J. Wang, X. W. Bu et al., "Adaptive fuzzy tracking control for constrained flexible air-breathing hypersonic vehicle based on actuator compensation," *International Journal of Advanced Robotic Systems*, vol. 13, no. 6, pp. 1–12, 2016.

[14] X. Bu and H. Lei, "A fuzzy wavelet neural network-based approach to hypersonic flight vehicle direct nonaffine hybrid control," *Nonlinear Dynamics*.

[15] B. Xu, F. Sun, Y. Pan, and B. Chen, "Disturbance observer based composite learning fuzzy control of nonlinear systems with unknown dead zone," *IEEE Transactions on Systems, Man, and Cybernetics: Systems*, 2016.

[16] X. Bu, X. Wu, J. Huang, Z. Ma, and R. Zhang, "Minimal-learning-parameter based simplified adaptive neural back-stepping control of flexible air-breathing hypersonic vehicles without virtual controllers," *Neurocomputing*, vol. 175, pp. 816–825, 2016.

[17] B. Xu, D. Yang, Z. Shi, Y. Pan, B. Chen, and F. Sun, "Online recorded data-based composite neural control of strict-feedback systems with application to hypersonic flight dynamics," *IEEE Transactions on Neural Networks and Learning Systems*, vol. PP, no. 99, Article ID 2743784, pp. 1–11, 2017.

[18] Z. D. Wilcox, W. MacKunis, S. Bhat, R. Lind, and W. E. Dixon, "Lyapunov-Based exponential tracking control of a hypersonic aircraft with aerothermoelastic effects," *Journal of Guidance, Control, and Dynamics*, vol. 33, no. 4, pp. 1213–1224, 2010.

[19] B. Xu, F. Sun, H. Liu, and J. Ren, "Adaptive Kriging controller design for hypersonic flight vehicle via back-stepping," *IET Control Theory & Applications*, vol. 6, no. 4, pp. 487–497, 2012.

[20] W. A. Butt, L. Yan, and S. K. Amezquita, "Adaptive integral dynamic surface control of a hypersonic flight vehicle," *International Journal of Systems Science*, vol. 46, no. 10, pp. 1717–1728, 2015.

[21] B. Xu, X. Huang, D. Wang, and F. Sun, "Dynamic surface control of constrained hypersonic flight models with parameter estimation and actuator compensation," *Asian Journal of Control*, vol. 16, no. 1, pp. 162–174, 2014.

[22] W. Dong, J. A. Farrell, M. M. Polycarpou, V. Djapic, and M. Sharma, "Command filtered adaptive backstepping," *IEEE Transactions on Control Systems Technology*, vol. 20, no. 3, pp. 566–580, 2012.

[23] R. Li, M. Chen, and Q. Wu, "Adaptive neural tracking control for uncertain nonlinear systems with input and output constraints using disturbance observer," *Neurocomputing*, vol. 235, pp. 27–37, 2017.

[24] K. Yong, M. Chen, and Q. Wu, "Constrained adaptive neural control for a class of nonstrict-feedback nonlinear systems with disturbances," *Neurocomputing*, vol. 272, pp. 405–415, 2018.

[25] B. Xu, S. Wang, D. Gao, Y. Zhang, and Z. Shi, "Command filter based robust nonlinear control of hypersonic aircraft with magnitude constraints on states and actuators," *Journal of Intelligent & Robotic Systems*, vol. 73, no. 1–4, pp. 233–247, 2014.

[26] H. An, J. Liu, C. Wang, and L. Wu, "Disturbance Observer-Based Antiwindup Control for Air-Breathing Hypersonic Vehicles," *IEEE Transactions on Industrial Electronics*, vol. 63, no. 5, pp. 3038–3049, 2016.

[27] M. Chen, S. S. Ge, and B. Ren, "Adaptive tracking control of uncertain MIMO nonlinear systems with input constraints," *Automatica*, vol. 47, no. 3, pp. 452–465, 2011.

[28] Q. Zong, F. Wang, B. Tian, and R. Su, "Robust adaptive dynamic surface control design for a flexible air-breathing hypersonic vehicle with input constraints and uncertainty," *Nonlinear Dynamics*, vol. 78, no. 1, pp. 289–315, 2014.

[29] Q. Zong, F. Wang, R. Su, and S. K. Shao, "Robust adaptive backstepping tracking control for a flexible air-breathing hypersonic vehicle subject to input constraint," *Proceedings of the Institution of Mechanical Engineers, Part G: Journal of Aerospace Engineering*, vol. 229, no. 1, pp. 10–25, 2015.

[30] Y. Fu, Y. Liu, and D. Huang, "Boundary output feedback control of a flexible spacecraft system with input constraint," *IET Control Theory & Applications*, vol. 12, no. 5, pp. 571–581, 2018.

[31] M. A. Bolender and D. B. Doman, "Nonlinear longitudinal dynamical model of an air-breathing hypersonic vehicle," *Journal of Spacecraft and Rockets*, vol. 44, no. 2, pp. 374–387, 2007.

[32] J. T. Parker, A. Serrani, S. Yurkovich, M. A. Bolender, and D. B. Doman, "Control-oriented modeling of an air-breathing hypersonic vehicle," *Journal of Guidance, Control, and Dynamics*, vol. 30, no. 3, pp. 856–869, 2007.

[33] B. Xu, Q. Zhang, and Y. Pan, "Neural network based dynamic surface control of hypersonic flight dynamics using small-gain theorem," *Neurocomputing*, vol. 173, pp. 690–699, 2016.

[34] X. Wang and H. Lin, "Design and frequency analysis of continuous finite-time-convergent differentiator," *Aerospace Science and Technology*, vol. 18, no. 1, pp. 69–78, 2012.